Scaling of the streamwise turbulence intensity in the context of inner-outer interactions in wall turbulence*

Ivan Marusic,† Woutijn J. Baars, and Nicholas Hutchins
Department of Mechanical Engineering, University of Melbourne, Melbourne, Victoria 3010, Australia
(Received 3 July 2017; published 17 October 2017)

The classical view of wall-bounded turbulence considers a near-wall inner region where all velocity statistics are universally dependent on distance from the wall when scaled with friction velocity and the kinematic viscosity of the fluid. This is referred to as an inner scaling and leads to Prandtl's law of the wall. Data from numerical simulations and experiments over the past decade or so, however, have provided compelling evidence that statistics of the fluctuating streamwise velocity do not follow inner scaling in this near-wall region and an interaction of outer and logarithmic regions exists, resulting in a Reynolds number dependence. In this paper we briefly review some of these studies and discuss the Reynolds number dependence of the streamwise turbulence intensity near the wall in terms of an inner-outer interaction. An established model for such an interaction between near-wall and logarithmic region turbulence is considered that comprises two mechanisms: superposition and modulation. Here outer-region motions, of which a fraction is wall-attached, are superimposed onto the near-wall dynamics, and concurrently the near-wall motions are modulated by this superimposed signature. We discuss to what extent the superposition effect can relate changes in the inner-scaled near-wall peak value of streamwise turbulence intensity to logarithmic region turbulence resembling features of attached eddies.

DOI: 10.1103/PhysRevFluids.2.100502

I. INTRODUCTION

This article is an invited contribution resulting from the Stanley Corrsin Award Lecture delivered by the first author at the 69th annual APS-DFD meeting in Portland, Oregon, USA, in 2016, on the topic of wall-bounded turbulent flows. Such flows are commonly encountered in many engineering, environmental, and geophysical applications, and therefore fundamental advances in our understanding of wall turbulence can possibly lead to broad impacts across a range of fields. Our paper, however, is not meant to be an exhaustive review, but rather, more a perspectives piece intended to give a summary of some of the authors' views presented during this lecture, and we extend the discussion to consider a spectral coherence analysis as presented recently by Baars *et al.* [1,2], focusing on the implications for scaling of the streamwise turbulence intensity due to inner-outer interactions.

Throughout this paper x, y, and z refer to the streamwise, spanwise, and wall normal directions, respectively, with u, v, and w representing the respective Reynolds decomposed velocity fluctuations. Quantities with overbars refer to time averages, while angled brackets indicate ensemble averaged quantities.

The Reynolds number of a turbulent boundary layer can be viewed as a measure of the range of scales present in the flow. The friction Reynolds number $\mathrm{Re}_\tau \equiv \delta U_\tau/\nu$ clearly embodies this, representing a ratio between δ (the boundary layer thickness) and the viscous length scale ν/U_τ, where ν is the kinematic viscosity and U_τ is the friction velocity. Here $U_\tau = \sqrt{\tau_o/\rho}$ where τ_0 is

*APS-DFD Stanley Corrsin Award.

†imarusic@unimelb.edu.au

the wall shear stress. At any given Re, the near wall represents the region in a turbulent boundary layer where the full range of scales will be most apparent. This is because an observation made at the wall sees not only the small-scale near-wall structures that reside in this region, but also a superposition of the larger u and v fluctuations originating from (attached) turbulent structures that may be centered much further from the wall. This behavior is evident from energy spectra at reasonably high Reynolds number, for example, in the spectrograms presented in Refs. [3,4].

The superposition of energy from a whole range of scales onto the near-wall region is now a reasonably well-accepted and expected consequence of a hierarchical distribution of coherent structures. This is also a central tenet of attached eddies in the sense of Townsend [5] or Perry and Chong [6], whereby a hierarchical distribution of attached representative eddies that are linearly superposed demonstrate a convincing description of many aspects of wall-bounded turbulence. Regardless of the precise form of the "representative eddy," attached eddy models all predict an increasing range of scales, and hence an increasing broadband u intensity in the near-wall region, as Reynolds number increases. This is in contrast to the classical description of near-wall turbulence, which assumes an inner region (say, $0 < z^+ < 30$) that is independent from the outer region, such that all time-averaged, inner-scaled, turbulence statistics can be expressed as universal functions of z^+. Clearly the increasing superposition of large-scale energy at high Reynolds numbers challenges this classical position, and indeed a large number of studies have demonstrated that this is not the case. Perhaps the clearest example is the growth in the near-wall peak of the broadband turbulence intensity of the u fluctuations with increasing Reynolds number.

Caution must be exercised when interpreting data at $z^+ \approx 15$ at high Reynolds numbers due to the spatial and temporal resolution challenges [7,8]. It is noted that at extremely high Reynolds numbers, studies in pressurised facilities do not seem to show growth in this inner peak [9,10], and this remains an open question. However, at $\mathrm{Re}_\tau \lesssim 30\,000$, there is now clear evidence that this occurs [8,11–18], and that this growth in the peak is due to a growing superposition of larger-scale energy from log and outer-region structures as Re increases [8,14,16]. Near-wall energy spectra, and instantaneous views of this region, have also long hinted at the superposition of a growing range of energetic scales as Re increases [3,4,19–21].

This superposition has some implications to the near-wall cycle of streaks and quasistreamwise vortices [22–24] that populate the near-wall region of turbulent boundary layers. The pioneering work in minimal channels by Jiménez and Pinelli [25] cemented the view that this cycle is "autonomous"; it does not require external triggers from outer larger-scale eddies to self-sustain. As this region has been probed at increasingly higher Reynolds numbers, a slightly refined view has emerged of a near-wall cycle, which, though perhaps not dependent on external triggers for self-sustenance, is increasingly coexisting within a sea of larger-scale superimposed energy as Re increases. Interestingly, in this near-wall region these footprints of larger-scale events have an effect beyond a purely linear superposition. It has been demonstrated through numerous experiments and simulations that the small-scale energy in the near-wall region is also amplitude and frequency modulated by the large-scale superimposed footprints. In the near-wall region, at least, this modulation is relatively well explained by a quasisteady argument [26]. In short, once the scale separation between the small scales and the larger superimposed scales is sufficient, we can assume that the small scales will "feel" the large-scale footprint as a modulated boundary condition, via an altered wall shear stress. For example, a large-scale positive u fluctuation will result in a large-scale quasisteady period of enhanced wall shear stress (analogous to an enhanced local Reynolds number) to which the near-wall structure and small scales will respond. As the local τ_0 increases, the near-wall viscous scaled events will respond such that their length, convection velocity, and fluctuation magnitude remain fixed in local inner scaling. When viewed in terms of a global scaling, this will lead to a locally enhanced amplitude and frequency of fluctuations during large-scale positive u fluctuations. This amplitude and frequency modulation of the near-wall small-scale events, a predicted result of the quasisteady assumption, has been described in a number of recent papers [26–29].

An enhanced understanding of the interaction between large- and small-scale events has permitted the formulation of models that can predict near-wall statistics based only on a knowledge of the large-scale fluctuations measured in the logarithmic region of the boundary layer. For example, the model put forward by Mathis *et al.* [30,31] assumes a universal near-wall signal (this universal signal is the near-wall cycle, free of superposition or modulation, effectively equivalent to low Reynolds number near-wall turbulence). The input large-scale fluctuation in the logarithmic region is used to amplitude modulate this universal signal (based on a modulation coefficient predetermined from a calibration experiment) and is also superimposed onto the modulated signal (with a magnitude given by a predetermined superposition coefficient). Such models have been demonstrated to provide reasonably reliable predictions of near-wall turbulent statistics at Reynolds numbers far removed from the Re of the calibration experiment. As well as permitting predictions of near-wall statistics in situations where such measurements would perhaps not be accessible, these models also provide a conceptual model of how scales interact in the near-wall region and how this is likely to evolve with Reynolds number.

In light of the above descriptions, and in particular their strong resonance with hypotheses relating to attached eddies, it is worth briefly mentioning here recent evidence that seems to explicitly demonstrate the existence of a hierarchical distribution of self-similar representative eddies. It is puzzling that even today the term "attached eddy" should invoke so much controversy in the field, when in the spirit of Townsend it was merely an attempt at proposing a distribution of representative eddies that *could* provide an explanation for observed correlation statistics. The emphasis here is on *could*; Townsend at no time seemed wedded to a particular characteristic eddy, and indeed changed this proposed eddy throughout his career. Much of the current controversy seems to revolve around the choice of this eddy, which, in many ways, seems of secondary importance compared to the concept that a hierarchical distribution of *some* wall-attached eddy can provide a useful and convincing description of many facets of wall-bounded turbulence. If we set aside arguments over the precise form of a representative eddy, recent evidence points to the presence of such a hierarchical distribution. Of note here is the review by Jiménez [32], who concludes that, using minimal channel results of Flores and Jiménez [33], the logarithmic law reflects a structure agreeing reasonably well with Townsend's model of a self-similar family of attached eddies. Through analysis of filtered and minimal channel simulations, Hwang [34] also made similar conclusions. In both cases the self-similar "representative" eddy seemed reminiscent of the self-sustaining process observed for the near-wall cycle by Jiménez and Pinelli [25] and Schoppa and Hussain [35]. Klewicki *et al.* [36] showed that a self-similar hierarchical structure is required for invariant solutions of the leading-order mean dynamics in the Navier-Stokes equations, and transient growth and resolvent analysis has also revealed self-similar behaviors (reviewed by McKeon [37]). Experimentally, Hellström *et al.* [38] have also reported (through proper orthogonal decomposition analysis of particle image velocimetry data) self-similar energetic modes in pipe flow. Baars *et al.* [1] make use of coherence spectra between a fixed near-wall probe and a probe traversing the outer region to uncover evidence of a self-similar wall-attached structure. Since this structure is inferred from coherence spectra alone, there are few available details of the representative eddy, other than a proposed aspect ratio of geometrical self-similarity. However, in general the stochastic representative eddies determined from experiments will tend to favor symmetrical representative eddies (typical of the double-roller eddy types originally proposed by Townsend, or the hairpin- or lambda-shaped vortices prevalent in recent literature [39,40]), while the recent advent of time resolved three-dimensional views of these features typically yield a representative eddy that evolves in time, exhibiting various asymmetries (cf. the self-sustaining process of Schoppa and Hussain [35]). The attached eddy framework, as originally put forward by Townsend, was an attempt to explain time-averaged statistics; however, recent papers [41,42] have demonstrated that a distribution of representative eddies can produce instantaneous features that qualitatively match observed instantaneous behavior in turbulent boundary layers regarding uniform momentum zones [43] and internal shear layers [44,45].

II. DEFINING FEATURES AT HIGH REYNOLDS NUMBER

A. Importance of the logarithmic region

While debate continues about the precise bounds of the logarithmic region in wall-bounded flows [46–48], it is agreed that high-Reynolds-number data are a prerequisite for validating logarithmic scaling behaviors in wall-normal profiles of the mean streamwise velocity and the streamwise turbulence intensity [18,49]. For instance, when assuming that the logarithmic region in a turbulent boundary layer (TBL) flow starts at an inner-scaled position of $z^+ \approx 100$, and ends at an outer-scaled position of $z/\delta \approx 0.15$, the log region would be nonexistent for $\mathrm{Re}_\tau \lesssim 670$. Moreover, $\mathrm{Re}_\tau \gtrsim 6700$ is required for the log region to span at least one decade in z. When adopting a more conservative lower bound for the log region as $z^+ = 3\mathrm{Re}_\tau^{1/2}$, following Sreenivasan and Sahay [50], Klewicki *et al.* [36], and Marusic *et al.* [49], one would require $\mathrm{Re}_\tau \gtrsim 40\,000$ for the log region to span one decade in z.

For investigations of how turbulence is (re)generated and sustained, the metric of turbulent kinetic energy production becomes insightful. In particular, a defining feature of an increasing scale separation with growing Re_τ is the relative contribution to the kinetic energy production from the different wall-normal regions [51,52]. Turbulent kinetic energy production is defined as the product of the Reynolds shear stress and mean shear,

$$P = -\overline{uw}^+ \frac{d\overline{u}^+}{dz^+}. \tag{1}$$

Figure 1(a) presents premultiplied profiles of the kinetic energy production, z^+P, for three values of Re_τ. In the semilogarithmic plot, the area under the curves is proportional to the global or bulk kinetic energy production. When analyzing the contributing fraction of P in the near-wall region (here taken as $0 < z^+ < 30$) to the bulk kinetic energy production (total area under the curves), it is evident that this contribution decreases with increasing Re_τ. This is shown by the dashed line in Fig. 1(b). Consequently, the contribution to the bulk production from the log region increases.

For relevance to engineering systems, where $\mathrm{Re}_\tau \sim O(10^4)$–$O(10^6)$, the main contribution to the bulk production comes from the log region. And so, the predominant kinematics and dynamics that drive the turbulence cascade in high-Reynolds-number wall-bounded turbulence occurs in the

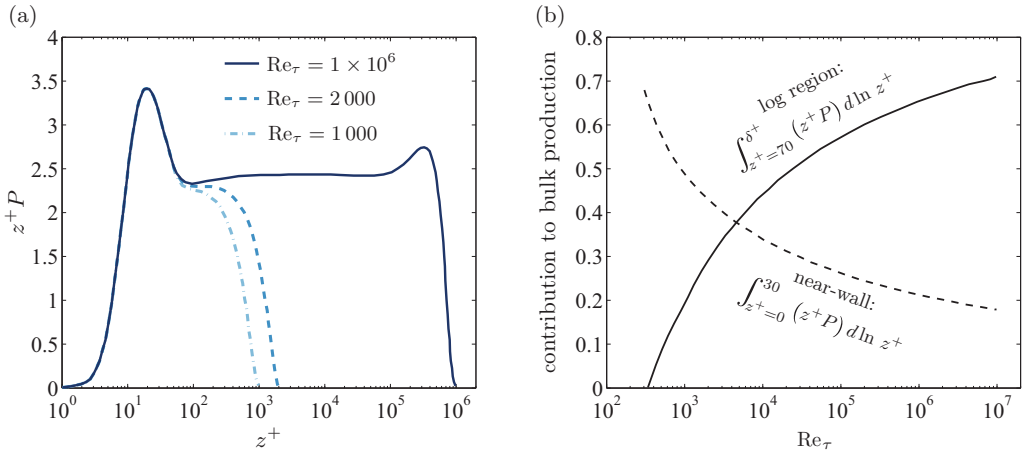

FIG. 1. (a) Premultiplied turbulence kinetic energy production, z^+P, for three values of Re_τ. Wall-normal profiles of P were estimated using the formulations for the mean velocity profile (law of the wall wake) and the corresponding Reynolds shear stress, following Perry *et al.* [53]. (b) Contributing fractions to the bulk kinetic energy production from the production P in the near-wall region (taken as $0 < z^+ < 30$) and the log region ($70 < z^+ < 0.15\,\mathrm{Re}_\tau$). Panels (a) and (b) were adapted from Ref. [51].

log region. It is furthermore known that the dynamics in the outer region impacts the smaller-scale dynamics in the near-wall region through a scale-interaction process. Therefore, the physical underpinning of the (self-sustaining) dynamics in high-Reynolds-number flows can be fundamentally different in comparison to lower-Reynolds-number flows, for which the self-sustaining near-wall cycle is the dominant driver. This was recently further confirmed by Renard and Deck [54], who showed that the bulk production of turbulent kinetic energy is directly reflected by the difference in mean skin friction between laminar and turbulent flows, and consequently at high Reynolds numbers the generation of the turbulence-induced excess friction is dominated by the logarithmic layer. They further conclude that this suggests that it may be worth investigating new drag reduction strategies focusing on turbulent kinetic energy production and on the nature of the logarithmic layer dynamics.

B. On the coherence along the wall-normal direction

An organization in high-Reynolds-number wall turbulence is most pronounced in the logarithmic region where large-scale turbulent structures comprise significant lifetimes in the streamwise direction [24,55]. This organization is often described via a classification of coherent structures [52], including hairpin vortices, large-scale motions, and very-large-scale motions (or superstructures [3]). In this section we focus on one explicit aspect of coherence in TBL flows: the portion of the turbulence in the outer region that is coherent with a very-near-wall reference position (covered in detail by Baars *et al.* [1]). This also serves as additional evidence for the direct linkage between outer-region turbulence and the near-wall fluid dynamics.

A consistent coupling within the wall-bounded turbulence can be inferred from two-point synchronized data. Here we consider one inner-region reference position at $z_I^+ \approx 4.4$ for a Reynolds number condition of $\mathrm{Re}_\tau \approx 14\,000$ [1]. It is instructive to compute the coupling between the outer-region turbulence (mapped out with synchronously acquired traversing probe) and the inner-region fluctuations in spectral space to obtain a scale-by-scale (linear) correlation, which is referred to as the linear coherence spectrum (LCS), defined as

$$\gamma_L^2(z,z_I;\lambda_x) \equiv \frac{|\langle U(z;\lambda_x)U^*(z_I;\lambda_x)\rangle|^2}{\langle |U(z;\lambda_x)|^2\rangle \langle |U(z_I;\lambda_x)|^2\rangle}. \tag{2}$$

Here $U(z;\lambda_x) = \mathcal{F}[u(z)]$ is the Fourier transform of $u(z)$. It is noted that the numerator equals the cross-spectrum magnitude squared, while the two energy spectra of $u(z_I)$ and $u(z)$ form the denominator. (Note that the asterisk indicates the complex conjugate, $\langle\rangle$ denotes ensemble averaging, and $||$ indicates the modulus.) Since γ_L^2 incorporates only the magnitude of the cross-spectrum, the value of γ_L^2 represents the maximum correlation for a specific scale (corresponding to a certain stochastically consistent phase shift of that scale, represented by the scale-dependent phase of the complex-valued cross-spectrum). Consequently, γ_L^2 equates to the fraction of common variance shared by $u(z_I)$ and $u(z)$ (note that $0 \leqslant \gamma_L^2 \leqslant 1$). Since one coherence spectrum is obtained for each $u(z_I)$-$u(z)$ combination, where z ranges from $z^+ \approx 10.5$ up to the free stream, we present the coherence as γ_L^2 iso-contours in Fig. 2. That is, the coherence spectrum for the streamwise velocity fluctuations at z_I and z_O is obtained by slicing the γ_L^2 contours at the outer-region position z_O. The coherence spectrogram is overlaid on the energy spectrogram of the streamwise velocity fluctuations, shown as iso-contours of the premultiplied form $k_x\phi_{uu}/U_\tau^2$. It is evident that only the larger scales remain coherent with the near-wall reference z_I when moving up throughout the outer region. Baars *et al.* [1] interpreted the trend in the iso-contours of γ_L^2 as a reflection of geometrically self-similar wall-attached structures, and we refer to that work for further details. In the triangular region bounded by an inner limit ($\lambda_x/z = 14$) and outer limit ($\lambda_x/\delta = 10$) a portion of the streamwise velocity fluctuations reflects this self-similar wall-attached eddy structure as envisioned by Townsend [5].

We now consider u fluctuations only at two locations along the wall-normal direction, denoted as $u(z_I)$ and $u(z_O)$ (referring to the inner and outer regions, respectively). In Fig. 3 we present three coherence spectra from two-point data of TBL flows. One curve corresponds to a direct

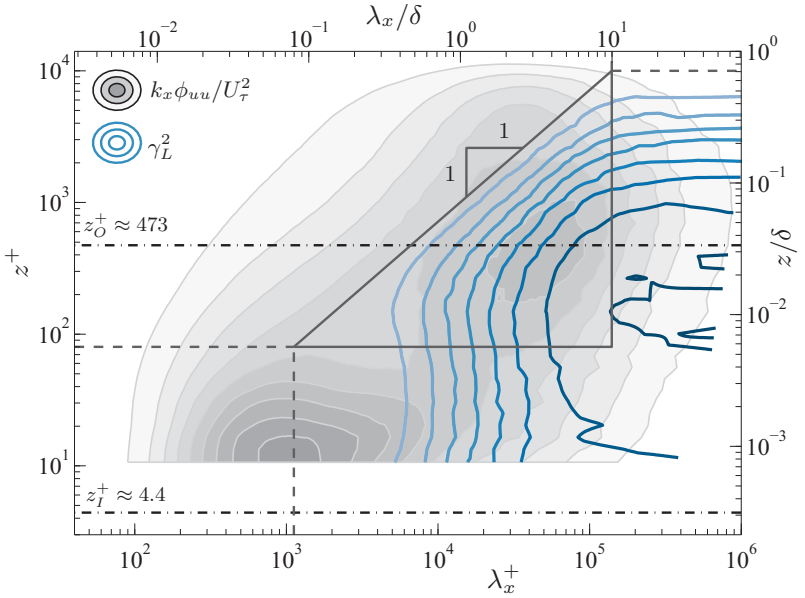

FIG. 2. Premultiplied energy spectrogram $k_x\phi_{uu}/U_\tau^2$ (levels: 0.2:0.2:1.8) at $\mathrm{Re}_\tau \approx 14\,000$ with an overlaid coherence spectrogram $\gamma_L^2(z,z_I;\lambda_x)$ relative to the reference location $z_I^+ \approx 4.4$ (levels: 0.1:0.1:0.9), following Baars *et al.* [1]. The hypotenuse of the triangle equates to $\lambda_x/z = 14$ and spans from $z^+ = 80$ up to $z/\delta \approx 0.71$ (the right-hand side is located at $\lambda_x/\delta = 10$).

numerical simulation (DNS) at $\mathrm{Re}_\tau \approx 2000$ [56], whereas the other two curves were generated from experimental data taken in Melbourne's boundary layer facility ($\mathrm{Re}_\tau \approx 14\,000$ [29], using two-point hot-wire anemometry) and data taken at the SLTEST facility in the atmospheric surface layer (ASL) ($\mathrm{Re}_\tau \approx 1.4 \times 10^6$ [57], using sonic anemometry above a wall-shear-stress sensor).

For all three data sets, the outer-region position was chosen as $z_O^+ \approx 3.9\mathrm{Re}_\tau^{1/2}$, following Mathis *et al.* [31], and resides within the logarithmic region (note that for the discussion that follows we could choose any outer position within the log region). A near-wall reference sensor at $z_I^+ \approx 4.4$ captured the near-wall u fluctuations for the $\mathrm{Re}_\tau \approx 14\,000$ case, which was considered in Fig. 2 (and a matching inner-scaled position of $z_I^+ \approx 4.3$ was taken in the DNS case). A purpose built wall-flush-mounted shear-stress sensor captured the wall-shear stress fluctuations for the $\mathrm{Re}_\tau \approx 1.4 \times 10^6$ flow. An increasing trend of the inner-outer coherence with increasing wavelength is apparent in all three data sets and collapses when the wavelength axis is normalized by the outer position, e.g., λ_x/z_O. Baars *et al.* [1] described this Reynolds number universality as the result of a self-similar structure embedded within the wall-attached turbulence, consistent with an attached-eddy structure conceptualized by Townsend [5]. The logarithmic increase in γ_L^2 was quantified with the expression in Fig. 3 and its corresponding trend line is shown in the figure [1]. The self-similar range of scales increases logarithmically with Re_τ. Coherence spectra for the full range of outer positions, relative to the near-wall reference position, suggest that a wall-attached and self-similar structure is ingrained in the u fluctuations for $\mathrm{Re}_\tau \sim O(10^3)$–$O(10^6)$. In (λ_x,z)-space, these u fluctuations reside within a region defined by an inner-scaling limit of $\lambda_x/z \approx 14$ and an outer-scaling limit of $\lambda_x/\delta \approx 10$; this region may appear down to a lower limit of $z^+ \approx 80$ (as indicated in Fig. 2 [1]).

At the large-wavelength end of Fig. 3, γ_L^2 spectra plateau to a magnitude that increases with Re_τ. This is caused by the transition from the self-similar increasing trend, to the scale-independent trend, which appears at $\lambda_x/\delta \approx 10$. For reference, the curves in Fig. 3 extend up to $\lambda_x \approx 12\delta$ (spatial DNS), $\lambda_x \approx 27\delta$ (Melbourne), and $\lambda_x \approx 34\delta$ (SLTEST). Note that for temporal data (Melbourne and SLTEST data) the frequencies were transformed to wavelengths using the local mean velocity

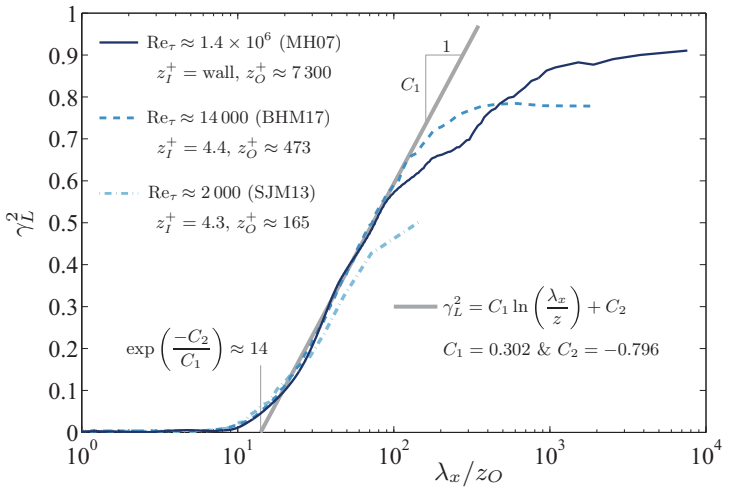

FIG. 3. Linear coherence spectra $\gamma_L^2(z_I, z_O, \lambda_x)$ between inner- and outer-region positions in a TBL flow (z_I and z_O, respectively), at three Re_τ conditions. Atmospheric surface layer data of (MH07) Marusic and Heuer [57], laboratory data of (BHM17) Baars, Hutchins, and Marusic [29], and DNS data of (SJM13) Sillero, Jiménez, and Moser [56]. Positions z_I and z_O are listed in the legend and described in the text. Note that the wavelength axis is presented as λ_x/z_O. The logarithmic increase in the coherence, per the expression in the figure, is described in the recent work by Baars, Hutchins, and Marusic [1].

at the outer position, $\overline{u}(z_O)$. A promising result of Fig. 3 and the study by Baars *et al.* [1] is that high-Reynolds-number flows include a larger range of energetic scales that are coherent in the wall-normal direction (relative to the total range of energetic scales). Again, this coherence reflects a self-similar structure of wall-attached turbulence and the existence of wall-coherent larger-scale motions [43]. The maximum coherence of $\gamma_L^2 \approx 0.9$ in the $\mathrm{Re}_\tau \approx 1.4 \times 10^6$ data is exceptionally high for two-point turbulence applications (note that the relatively poor transition from the self-similar trend to the plateau at large λ_x/z_O is caused by difficulties in accurately capturing the very large-scale motions in the ASL, e.g., due to the variation in free-stream velocity and issues of convergence).

Moving forward, the illustrated aspect of strong coherence along the wall-normal direction may be used for a linear stochastic estimate (LSE) of the turbulence [58]. For a single-input or -output system, a stochastic estimate evaluates a conditional output from an unconditional input, via a stochastic transfer kernel. When performing the estimate in spectral space [59], a complex-valued linear transfer kernel H_L captures how the output is stochastically coupled with the input, for each Fourier scale (linear). When taking $u(z_O)$ as input, and $u(z_I)$ as output, the kernel is defined as

$$H_L(z_I, z_O; \lambda_x) \equiv \frac{\langle U(z_I; \lambda_x) U^*(z_O; \lambda_x) \rangle}{\langle |U(z_O; \lambda_x)|^2 \rangle} = |H_L| e^{j\phi}. \tag{3}$$

Here the gain squared is related to the LCS of Eq. (2) via the ratio of the output-input energies, following

$$|H_L(z_I, z_O; \lambda_x)|^2 = \gamma_L^2(z_I, z_O; \lambda_x) \frac{\langle |U(z_I; \lambda_x)|^2 \rangle}{\langle |U(z_O; \lambda_x)|^2 \rangle}, \tag{4}$$

whereas phase ϕ of Eq. (3) embeds the scale-dependent stochastic phase shift for all coherent scales. A time-domain estimate $\widehat{u}(z_I)$ is now found from the inverse Fourier transform of the spectral LSE, according to

$$\widehat{u}(z_I) = \mathcal{F}^{-1}[\widehat{U}(z_I; \lambda_x)], \quad \text{where } \widehat{U}(z_I; \lambda_x) = H_L(z_I, z_O; \lambda_x) \mathcal{F}[u(z_O)]. \tag{5}$$

Here the spectral estimate consists of a single multiplication of the kernel and the Fourier-space representation of the unconditional input. During estimation, all coherent scales are thus weighted properly via the gain, while the scale-dependent phase efficiently accounts for the correct stochastic shift (and thus accounts for the well-known inclination of the larger, coherent scales in TBL flows; see, e.g., Refs. [57,60]). Baars *et al.* [29] presents an illustration of the conditional output of the boundary layer fluctuations via such a procedure. In the context of inner-outer interactions, the strong coherence—and thus the applicability of a spectral LSE for predicting the coherent scales—warrants its use in the inner-outer interaction model [2,30,31], which is reviewed next.

C. A review and illustration of the inner-outer interaction model

For any input-output system, a strong (linear) coherence opens avenues for predictive models. Here we revisit the inner-outer interaction model (IOIM) introduced by Marusic *et al.* [30] (details given in Refs. [26,61]). Streamwise velocity fluctuations at an outer-region position, z_O, form the input, while the u fluctuations at positions in the inner region are considered as outputs. In practice, such a predictive model may be used for generating turbulence statistics near the wall in high-Reynolds-number experiments, where sensor limitations pose measurement restrictions, or as a wall-model in large eddy simulations [62]. The model elucidates the inner-outer interaction (or input-output relation) as a twofold process, in which the two components are identified as *superposition* and *modulation*. An expression for the model via the recently refined description by Baars *et al.* [2] is given as

$$u_p^+(z^+,t^+) = \underbrace{u^*(z^+,t^+)\{1+\Gamma(z^+)\widehat{u}^+(z^+,t^+)\}}_{\text{modulation}} + \underbrace{\widehat{u}^+(z^+,t^+)}_{\text{superposition}}, \tag{6}$$

where $\widehat{u}^+$ is constructed via the spectral LSE procedure mentioned in Sec. II B, so

$$\widehat{u}^+(z^+,t^+) = \mathcal{F}^{-1}[\widehat{U}^+(z^+;\lambda_x)], \quad \text{where } \widehat{U}^+(z^+;\lambda_x) = H_L(z^+,z_O^+;\lambda_x^+)\mathcal{F}[u^+(z_O^+,t^+)]. \tag{7}$$

Here the time dependence, t, can also be a spatial dependence. In Eqs. (6) and (7), $u^*(z^+,t^+)$, $\Gamma(z^+)$ and $H_L(z^+,z_O^+;\lambda_x^+)$ are given parameters of the IOIM and are found from a two-point calibration experiment. Hence, the input to the IOIM—for a given Re_τ—is the viscous-scaled fluctuating signal $u^+(z_O^+,t^+)$ in the logarithmic (outer) region, generally taken at $z_O^+ = 3.9\mathrm{Re}_\tau^{1/2}$ following Mathis *et al.* [31]. Aside from the predictive capability, the model provides a simple but robust description of the inner-outer interactions between the near-wall and outer-region turbulence. We now proceed with an illustrative review of both the superposition and modulation term in Eq. (6) and highlight their physical underpinning.

1. *Superposition component of the IOIM: Stochastic estimation*

Superposition entails the linear coherence as reviewed in Sec. II B. That is, a portion of the near-wall fluctuations at an inner-region position z^+ that is coherent with the outer-region fluctuations at z_O^+ can be predicted via the spectral LSE procedure. The accuracy of the estimate (in terms of energy) is described by the coherence curve $\gamma_L^2(z^+,z_O^+;\lambda_x)$. For small wavelengths, $\gamma_L^2 \approx 0$, meaning that energy at these scales is not included in an LSE. These coherent scales need to be modeled and are included in the modulation term (Sec. II C 2). At the large wavelength end of the spectrum, γ_L^2 plateaus (e.g., to $\gamma_L^2 \approx 0.8$ for the $\mathrm{Re}_\tau \approx 14\,000$ curve in Fig. 3). Hence, at the larger scales the stochastically estimated fluctuations at z^+, denoted as $\widehat{u}^+(z^+,t^+)$, comprise a $\sim$0.8 fraction of the energy residing at these scales.

In the original formulation of the IOIM [30,31], the superposition component was formed by imposing a predefined energy portion of the outer-region signal (energetic scales residing at $\lambda_x^+ > 7000$) onto the z^+ position. In this procedure the large-scale outer-region signal was scaled by a single gain factor and shifted by a single time shift to account for the wall-normal inclination of the large-scale structures in wall turbulence (recall that the input-output locations are separated only in

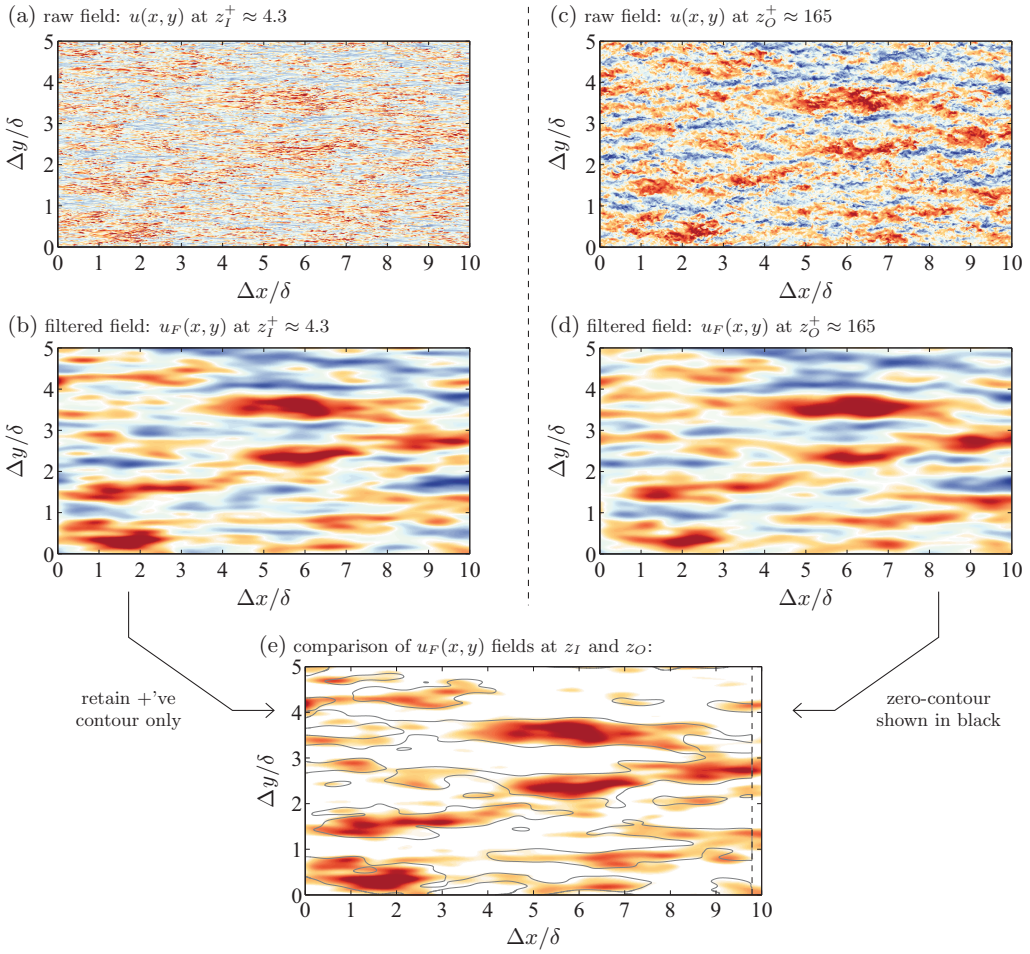

FIG. 4. Illustrating the superposition in the IOIM: coherence between the large-scale structures in the near-wall region and the outer region. (a) Streamwise velocity fluctuations in the wall-parallel plane at $z_I^+ \approx 4.3$. Data are from the DNS of Sillero *et al.* [56] at $\mathrm{Re}_\tau \approx 2000$. (c) Similar to (a) but with the filtered fluctuations; the long-wavelength pass filtering procedure is described in the text. (b, d) Similar to (a, b) but for a wall-normal location of $z_O^+ \approx 165$. (e) Match between the filtered fields in the inner and outer regions. All contours range from -3 (negative: blue) to $+3$ (positive: red) standard deviations of each respective field.

the z direction). This original procedure condenses to single-time LSE; Baars *et al.* [2] reviews that spectral LSE (or multi-time LSE) has a few inherent advantages over single-time LSE, since the scaling and shifting procedures are efficiently performed per Fourier scale with one multiplication in spectral space (Eq. 7). Moreover, the manual choice of the predefined energy portion (e.g., $\lambda_x^+ > 7000$) is eliminated since the scale-dependent gain in the spectral LSE results in an estimation of the coherent scales only (a data-driven method).

In summary, the superposition component forms the portion in the prediction, $u_p^+(z^+,t^+)$, that is linearly coherent with the input turbulence. Thus, superposition in the IOIM refers to a stochastic estimation (commonly applied to extract a coherent structure; see Refs. [63–69] among others). An illustration of the coherence between the inner and outer regions of a TBL flow is shown in Fig. 4. Streamwise velocity fluctuations in two wall-parallel planes at $z_I^+ \approx 4.3$ and $z_O^+ \approx 165$, are shown in Figs. 4(a) and 4(c), respectively. Note that the amplitude of the contour spans -3 to $+3$ standard deviations of the respective field shown (applies to all fields shown in Figs. 4 and 5). These data are

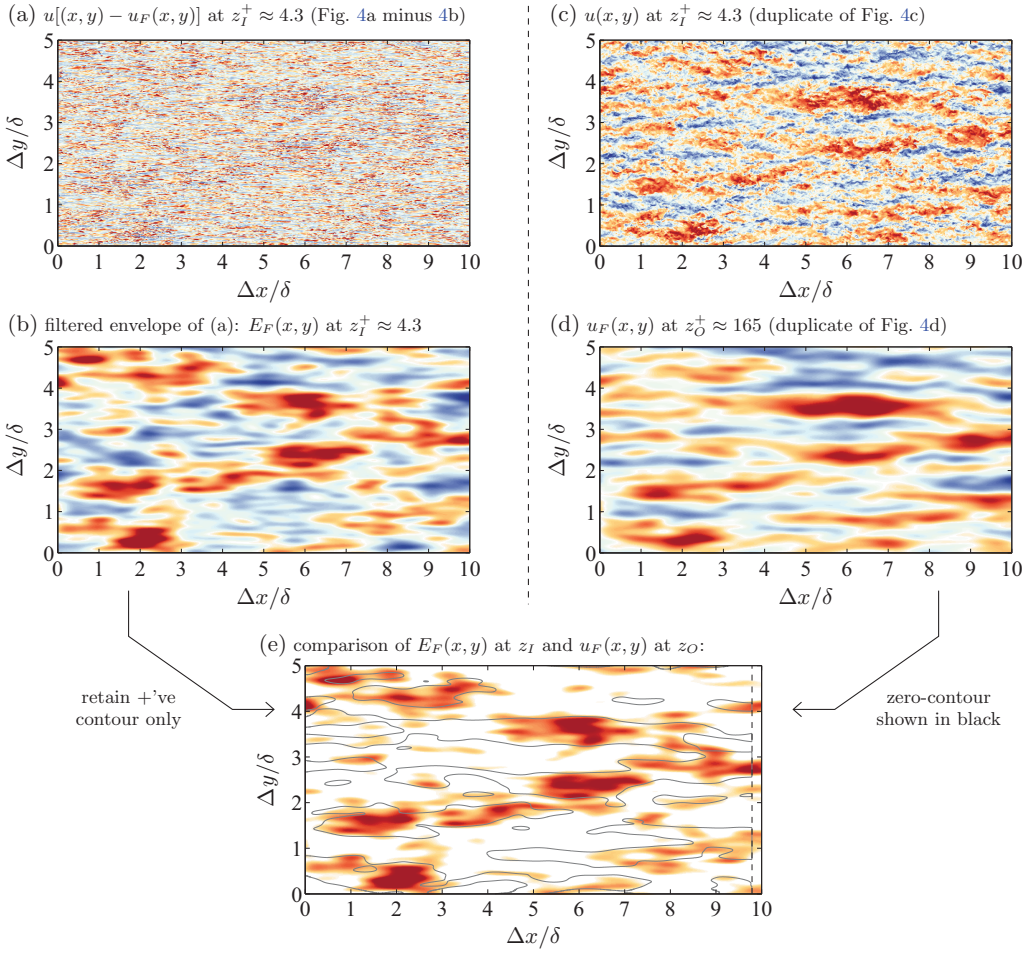

FIG. 5. Illustrating the modulation in the IOIM: modulation of small-scale near-wall structures by the larger scales that are coherent with the outer-region (e.g., modulation of universal scales by the superposition component). (a) Short-wavelength pass filtered streamwise velocity fluctuations in the wall-parallel plane at $z_I^+ \approx 4.3$, identical to $u(x,y) - u_F(x,y)$, the raw and long-wavelength pass filtered fields are shown in Figs. 4(a) and 4(b), respectively. (b) Long-wavelength pass filtered field of the envelope of the fluctuations shown in (a). Recall that the fluctuations in (a) do not comprise energy at these long wavelengths, but a long-wavelength variation appears in the envelope of the fluctuations (e.g., modulation). (c, d) Duplicates of Figs. 4(c) and 4(d). (e) Match between the envelope of the smaller scale fluctuations at z_I^+ and the filtered field in the outer region. All contours range from -3 (negative: blue) to $+3$ (positive: red) standard deviations of each respective field.

taken from the same DNS data [56] as used in Fig. 3; $\mathrm{Re}_\tau \approx 2000$ at the streamwise center of the $\Delta x = 10\delta$ long domain.

To highlight the coherent nature of the raw velocity fields $u(x,y)$ at z_I and z_O, both fields are filtered with a long-wavelength pass filter in λ_x space and subsequently in λ_y space. The filter in λ_x is taken as the coherence function $\gamma_L^2(z_I, z_O; \lambda_x)$ of Fig. 3. The same LCS is used for the subsequent filtering procedure in the spanwise direction, but with an aspect ratio of $\lambda_x = 3\lambda_y$ (characteristic for hairpin vortex packets [34]). Although the two-dimensional LCS can be computed in (λ_x, λ_y) space from the DNS data [70], rescaling the λ_x-dependent LCS with an aspect ratio of $\lambda_x = 3\lambda_y$ is justified here since this serves an illustrative purpose only. Filtered inner- and outer-region fields $u_F(x,y)$ are shown in Figs. 4(b) and 4(d). Since the long-wavelength pass filter retains only the

coherent portions of the fluctuations, these two fields are strongly correlated to a degree represented by γ_L^2 (thus with a correlation of $\approx$0.5 at the largest streamwise scales on the order of the 10δ long domain; see Fig. 3). In physical space this degree of coherence is illustrated in Fig. 4(e), where the positive fluctuations of the inner field are reshown with an overlaid zero contour of the fluctuations in the outer region. Note that the latter is shifted backwards (towards smaller x) to account for the inclination of the coherent structures. Per the discussion in Sec. II B, the coherence between z_I and z_O becomes stronger with increasing Re_τ and spans a larger range of the energetic scales. Therefore, if Fig. 4(e) would be available for ASL data, the match of the inner and outer fields would be even more pronounced.

2. *Modulation component of the IOIM: Scale interaction of universal scales*

Only the coherent scales between the prediction (z^+) and input (z_O^+) locations are included in the superposition component of Eq. (6). Incoherent scales cannot be estimated and have to be modeled. In the modulation term of Eq. (6), $u^*(1+\Gamma\widehat{u}^+)$, the viscous-scaled velocity fluctuations u^* (superscript $+$ is omitted for convenience) are stochastically *incoherent* with z_O^+ and are fused with the *coherent* superposition imprint during the prediction. Physically, the universal signal is envisioned as the inner-scaled velocity fluctuations that would exist at the prediction location in the absence of any imposed dynamics from the outer region. In a trail of observations it was identified that a scale interaction exists between the larger (coherent) scales and the smaller (incoherent) scales [4,16,19,29,71]. Close to the wall this interaction appears as an amplitude modulation (AM), meaning that the amplitude of the small-scale velocity fluctuations comprise a large-scale varying component, which is proportional to the large-scale velocity fluctuations (for details see Refs. [1,61]).

An illustration of the modulation is shown in Fig. 5. That is, Fig. 5(a) presents the short-wavelength pass filtered field of the u fluctuations at z_I^+, which is constructed by removing the long-wavelength pass filtered field from the raw fluctuations: e.g., the difference between $u(x,y)$ in Fig. 4(a) and $u_F(x,y)$ in Fig. 4(b). Hence, there is no energy in $[u(x,y)-u_F(x,y)]$ at the long wavelengths. However, the variation in the amplitude of the small-scale fluctuations does include a large-scale component, which is visualized in Fig. 5(b). First, an envelope to the u fluctuations in Fig. 5(a) is constructed via a Hilbert transform [61] or wavelet transform [72] technique (note that Agostini *et al.* [73] highlighted that this modulation is asymmetric in nature). This envelope field is long-wavelength pass filtered to construct the $E_F(x,y)$ field shown in Fig. 5(b). Clearly, large-scale regions exist where the small-scale fluctuations are more intense $[E_F(x,y)>0]$ than the average intensity in Fig. 5(a), and likewise, regions exist where the small-scale fluctuations are damped relative to their average intensity $[E_F(x,y)<0]$. The modulation envelope is strongly correlated with the superposition signature (closely resembling the filtered field in the outer region) as is illustrated with the overlaid fields in Fig. 5(e). Physically the near-wall modulation can be described with a quasisteady, quasihomogeneous framework, in which the smaller-scale motions in the near-wall region respond to the superposition of larger-scale fluctuations as if they are subject to a local Reynolds number change (see Refs. [1,27]).

During the construction of the universal signals $u^*(z^+,t^+)$ from a calibration data set, the ingrained AM is removed (details are described elsewhere [2,31]). When a prediction is made via Eq. (6), signal u^* is modulated with the superposition component via the term $(1+\Gamma\widehat{u}^+)$. Here Γ is a coefficient prescribing the AM strength. Note that the modulation factor does not influence even order moments of u_p^+ (thus the energy distribution and turbulence intensity are unaffected). Odd-order moments, however, such as the skewness, are affected by modulation [31].

To summarize, for smooth-wall flows, an IOIM has been able to accurately predict streamwise velocity fluctuations in the inner region of wall-bounded flows, given an outer-region input [2,30,31]. The predictions generate statistically representative signals, meaning that they comprise the correct energy spectrum and even- and odd-order moments. Energetic scales included in the superposition signature furthermore include the correct phase information at the near-wall position, directly induced from the outer-region input and the LSE procedure. It is unavoidable that the phase information of the

incoherent, universally modeled scales is irrelevant, due to their incoherent nature over the typical wall-normal separation distances employed in the IOIM (e.g., $|z_O^+ - z_I^+|$). Mathis *et al.* [26] has shown that the IOIM could also be used for predicting fluctuating signals of the wall-shear stress. Under specific conditions, and with new sets of calibration parameters, the model is also applicable to rough-walled flows [74,75].

III. IMPLICATIONS FOR SCALING OF THE STREAMWISE TURBULENCE INTENSITY

With the framework of the IOIM in mind, this section focuses on the scaling of the streamwise turbulence intensity in zero-pressure gradient TBL flows. In particular the scaling of the inner peak is discussed, in relation to the logarithmic decay in the outer region. Scaling laws and associated models for the streamwise turbulence intensity are to date still an active research subject and topic of debate (see overviews in Refs. [48,76,77], among others).

A. Experimental data and corrections for spatial resolution

Wall-normal profiles of the streamwise velocity fluctuations in fully developed ZPG TBL flows were acquired in Melbourne's boundary layer facility. One set of hot-wire anemometry data is documented in table 2 of Marusic *et al.* [78] and includes 10 Reynolds numbers ranging from $\mathrm{Re}_\tau \approx 2800$ to 13 400. Another set of data used in this section comprises five Reynolds numbers in the range of $\mathrm{Re}_\tau \approx 2800$ to 19 000, documented in Hutchins *et al.* [8].

For two Reynolds numbers, wall-normal profiles of $\overline{u^2}^+$ are shown against the outer-scaled wall-normal coordinate, z/δ, in Fig. 6. Raw data are presented with the dashed-line profiles, which were acquired using hot wires with a viscous-scaled length of $l^+ \approx 26.1$ and $l^+ \approx 22.7$, for the $\mathrm{Re}_\tau \approx 2800$ and 13 400 data, respectively. Since such a typical hot-wire sensor length results in an attenuation of the resolved energy $\overline{u^2}^+$, a correction scheme described by Smits *et al.* [79] is applied to all data. Streamwise turbulence intensity profiles corrected for the limited spatial resolution are presented with the solid lines in Fig. 6. All profiles shown in the remainder of this section are corrected in a similar manner. Preliminary work with Princeton NSTAP probes (miniature hot wires) in Melbourne's boundary layer facility confirms that the correction scheme and the scaling behaviors to be described next (Sec. III B) are valid for the Re_τ range considered in this paper. These new measurements were fully resolved (without any sensor attenuation) since the hot-wire length was $l^+ \lesssim 3.5$, which is similar to typical spanwise resolutions used in DNS studies.

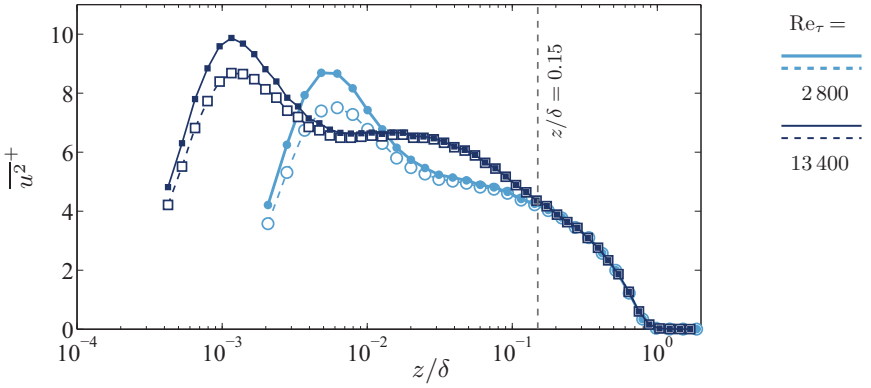

FIG. 6. Streamwise turbulence intensity profiles acquired in Melbourne's boundary layer facility [78] with (solid lines) and without (dashed lines) corrections for limited spatial resolution of the hot wire.

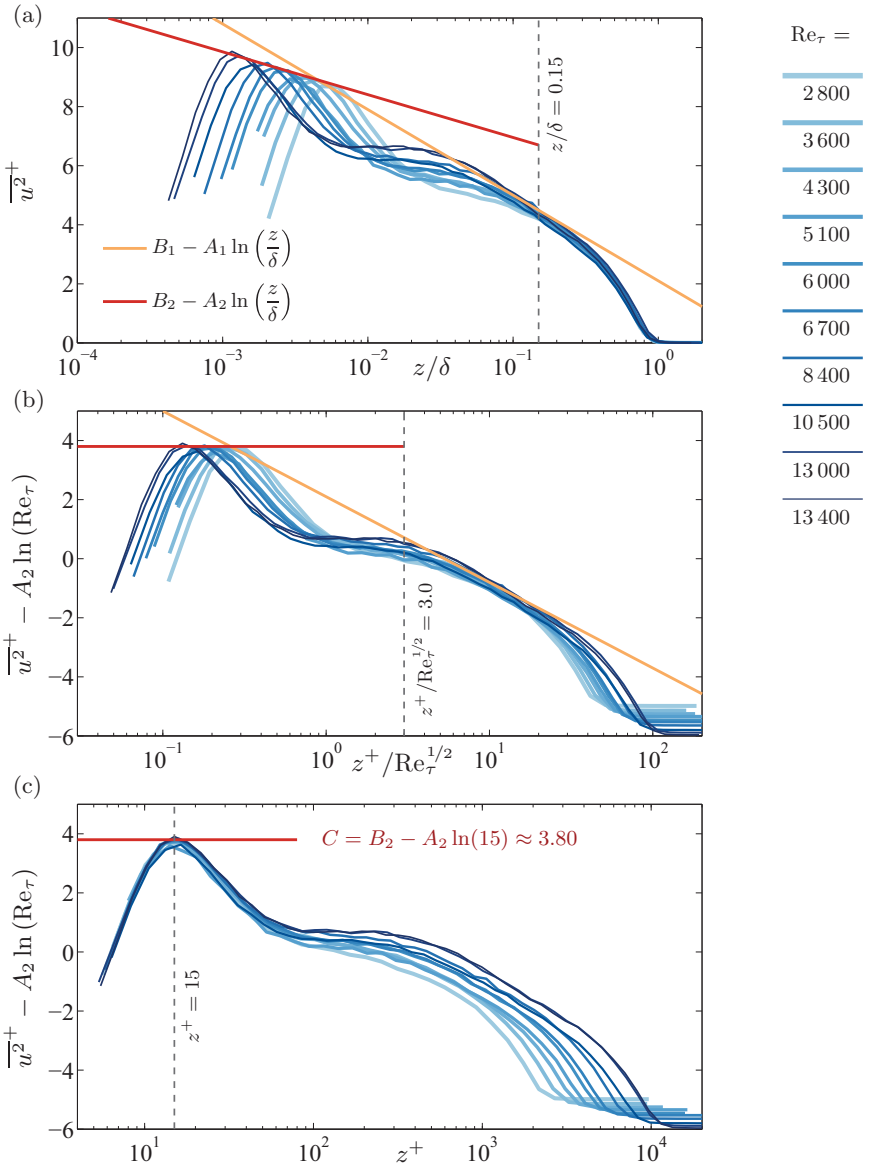

FIG. 7. Streamwise turbulence intensity profiles acquired in Melbourne's boundary layer facility [78], corrected for limited spatial resolution. The subfigures sequentially employ an (a) outer, (b) log, and (c) inner scaling of the wall-normal coordinate on the abscissae. Here $A_2 = A_1/2 = 0.63$, $C = 3.80$, and hence $B_2 = 5.51$ (see description in the text).

B. Scaling of the streamwise turbulence intensity in the inner and outer regions

For the data comprising the 10 Reynolds numbers [78], wall-normal profiles of $\overline{u^2}^+$ are shown as a function of z/δ in Fig. 7(a). A trend line for the logarithmic behavior in the outer region, following

$$\overline{u^2}^+ = B_1 - A_1 \ln\left(\frac{z}{\delta}\right), \tag{8}$$

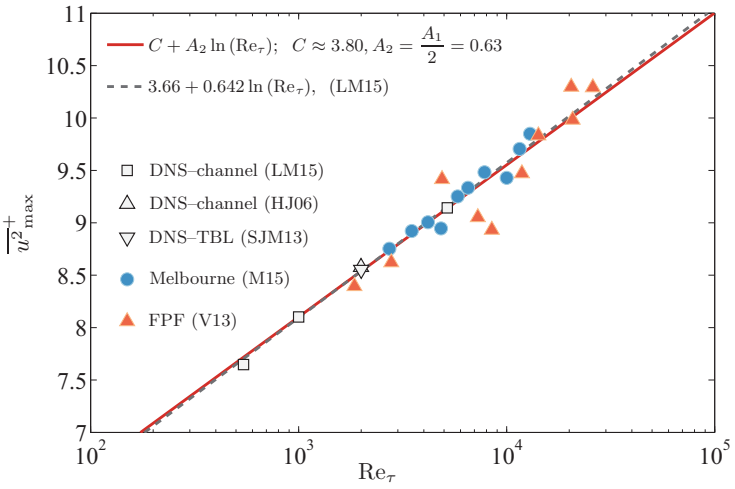

FIG. 8. Peak in the streamwise turbulence intensity, $\overline{u^2}^+_{\max}$, as a function of Re_τ. DNS data of (LM15) Lee and Moser [17] at $\mathrm{Re}_\tau \approx 550$, 1000, and 5200 (channel), (HJ06) Hoyas and Jiménez [16] at $\mathrm{Re}_\tau \approx 2000$ (channel), and (SJM13) Sillero, Jiménez, and Moser [56] at $\mathrm{Re}_\tau \approx 2000$ (TBL). Experimental data of (M15) Marusic *et al.* [78], acquired in Melbourne's boundary layer facility, and of (V13) Vincenti *et al.* [81], acquired in the Flow Physics Facility (FPF).

captures the data reasonably well around $z/\delta = 0.15$. Here $A_1 = 1.26$ [49] and the additive constant is taken as $B_1 = 2.10$. Maxima of the streamwise variance appear in the near-wall region, nominally at $z^+_{\max} \approx 15$ for ZPG TBL flows. Therefore, the peak in the variance profiles marches to lower values of z/δ when Re_τ increases. Consistent with previous studies [8,12,80] the magnitude of the inner peak $\overline{u^2}^+_{\max}$ increases with Re_τ. A logarithmic curve [note the semilogarithmic axes in Fig. 7(a)], similar to Eq. (8) but now with constants A_2 and B_2 via

$$\overline{u^2}^+_{\max} = B_2 - A_2 \ln\left(\frac{z_{\max}}{\delta}\right), \tag{9}$$

is seen to agree well with the data. This logarithmic trend was recently observed by Lee and Moser [17] who performed DNS channel flow up to $\mathrm{Re}_\tau \approx 5200$. When Eq. (9) is rearranged to a Reynolds number dependence while accepting that $z^+_{\max} \approx 15$, we obtain that the peak variance adheres to

$$\overline{u^2}^+_{\max} = B_2 - A_2 \ln(15) + A_2 \ln(\mathrm{Re}_\tau) = C + A_2 \ln(\mathrm{Re}_\tau). \tag{10}$$

Peak values of the streamwise variance as a function of Re_τ are shown in Fig. 8. DNS channel data of Lee and Moser [17] are considered, as well as the DNS channel data of Hoyas and Jiménez [16], which matches the TBL DNS data point of Sillero *et al.* [56]. Experimental TBL data from Melbourne correspond to Fig. 7(a), and the additional data shown were taken at the Flow Physics Facility (FPF), reported by Vincenti *et al.* [81], where, again, the $\overline{u^2}^+_{\max}$ values are corrected for spatial resolution using the scheme of Smits *et al.* [79]. Lee and Moser [17] reported Eq. (10) with $C = 3.66$ and $A_2 = 0.642$, shown with the dashed line in Fig. 8. We here recognize that a slope of $A_2 = A_1/2 = 0.63$ represents the trend in the data equally well; this is shown by the fitted solid line. The additive constant for the latter trend line was determined by fitting Eq. (10) with $A_2 = A_1/2$ to the five DNS data points, resulting in $C \approx 3.80$ (and $B_2 \approx 5.51$). A hypothetical discussion of how A_2 may be related to the logarithmic behavior in the outer region, captured by A_1, is provided in Sec. III C. Recall that the profiles in Fig. 7 and the associated peak values in Fig. 8 are obtained after correcting the raw data for the limited hot-wire spatial resolution (Sec. III A). Since Marusic

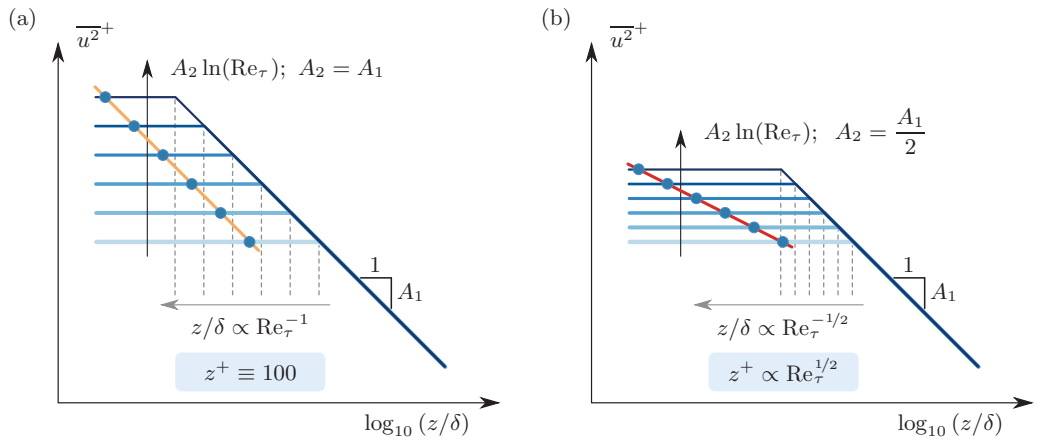

FIG. 9. Sketch of streamwise turbulence intensity profiles following a simplified attached eddy model. Each subsequent profile is subject to an equal increment in Re_τ; an increasing intensity corresponds to increasing Re_τ, and the same values of Re_τ are envisioned in panels (a) and (b). (a) The smallest attached eddy scales in viscous units ($100\nu/U_\tau$), and in (b) it scales with $\mathrm{Re}_\tau^{1/2}$. The orange and red lines track $z^+_{\max} = 15$.

et al. [78] performed the fit of Eq. (9) to the raw data, constants A_2 and B_2 reported here have changed.

Figure 7(b) further emphasizes the scaling behavior of the inner peak by showing the streamwise variance, minus $A_2 \ln(\mathrm{Re}_\tau)$ (Fig. 7 employs $A_2 = A_1/2 = 0.63$, $C = 3.80$, and $B_2 = 5.51$). With this ordinate the peaks in the streamwise variance follow the horizontal line at $C = 3.80$. Note that the wall-normal axis is presented in terms of a log-scaling, following $z^+/\mathrm{Re}_\tau^{1/2}$, to highlight that the outer-region scaling (Eq. 8) roughly holds up to a lower limit $z^+ \propto \mathrm{Re}_\tau^{1/2}$. Finally, Fig. 7(c) is similar to Fig. 7(b) but with an inner scaling of the wall-normal coordinate. Not just the peak variance shows excellent collapse, but the profiles collapse for a great extent of the near-wall region, e.g., $z^+ \lesssim 30$, suggesting that there is a universality of the inner peak in the absence of an energy contribution that grows logarithmically with Re_τ following Eq. (9). The outer-region superposition of energy onto a universal inner peak is addressed next.

C. Relating the inner peak scaling to the logarithmic behavior in the outer region

According to the classical model of an attached eddy structure, sketched out by Perry and Chong [6], the wall-normal extent of the smallest attached eddy scales with inner variables, e.g., $100\nu/U_\tau$. Subsequently, when the outer-region streamwise variance follows Eq. (8), an increasing Re_τ should result in an increase of the streamwise variance in the near-wall region (e.g., the increase of the peak variance) following Eq. (9) with $A_2 = A_1 = 1.26$. Here it is assumed that the streamwise variance in the outer region is superposed onto a viscous-scaled universal inner-peak in a one-to-one fashion (in other words, all energy is superposed without any "leakage"). This represents the classical view of the geometrically self-similar hierarchy of inertia-dominated motions, spanning $z^+ = 100$ to $z \sim \delta$ [schematically shown in Fig. 9(a)]. Clearly, the data in Fig. 7 do not support this.

In the classical view the smallest attached eddy coincides with the start of a logarithmic region [5]. An alternative view is that the smallest attached eddy scales with a lower bound of the logarithmic region according to $z^+ \propto \mathrm{Re}_\tau^{1/2}$ (see Sreenivasan and Sahay [50], Klewicki *et al.* [36], and Marusic *et al.* [49]). In that case a growth in Re_τ results in an increase of the streamwise variance in the near-wall region via Eq. (9) with $A_2 = A_1/2 = 0.63$; this case is sketched in Fig. 9(b). The data in Fig. 7 seem to support this model. However, in both these simplistic views of the classical attached eddy model [Figs. 9(a) and 9(b)], only the *total* streamwise turbulence intensity is considered (thus the integrated energy over *all* scales). Equation (8) describes the scaling of the cumulative energy.

The underlying assumption that all energetic scales in the outer region are one-to-one attached to the wall conflicts with the results reviewed in Sec. II B, which showed that only portions of the energy residing at scales $\lambda_x/z \gtrsim 14$ in the outer region are linearly coupled with the near-wall region [1]. To summarize, the turbulence in the outer region that is not coherent with the wall (generally the smaller-scale motions) adds to the total energy in the outer region, but is not superposed onto the wall (at least not via a linear coherent and stochastic mechanism). On the contrary, the attached eddy model accounts for only wall-attached (wall-coherent) contributions. It is therefore necessary to investigate the attached nature of the turbulence, and the associated scaling relations of the outer and inner regions [Eqs. (8) and (9)] as a function of scale; for this we go to spectral space.

As reviewed in Sec. II C, Baars *et al.* [2] formulated the superposition component of the IOIM [30,31] in terms of an LSE procedure. This guaranteed that the superposed fluctuations at an inner-region position z_I^+, from an outer-region input z_O^+, contain only the *linearly coherent* fluctuations between these two positions (and strictly speaking only for the Re_τ corresponding to the calibration experiment from which the kernel is found: $\mathrm{Re}_\tau \approx 13\,300$ [2]). All streamwise velocity fluctuations at z_I^+ that are *incoherent* with z_O^+ were modeled with u^* (recall Sec. II C 2). As is assumed in the IOIM, all incoherent (smaller) scales are universal in viscous scaling: this makes the contribution to $\overline{u^2}^+_{\max}$ from the modeled fluctuations invariant with Re_τ. Consequently, the scaling behavior of $\overline{u^2}^+_{\max}$ with Re_τ is envisioned to originate from the superposition component alone [8,14,16].

In order to examine the spectral energy contribution to $\overline{u^2}^+_{\max}$, due to superposition of outer-region energy, we consider $z_I^+ = z^+_{\max} \approx 15$. When formulating the energy spectrum of the spectral estimate (superposition) in Eq. (7), we can formulate the superposition contribution to the inner-peak variance as

$$\overline{u^2}^+_{\max}\Big|_{\text{superposition}} = \int \underbrace{|H_L(z^+_{\max}, z_O^+; \lambda_x^+)|^2 \Big[\frac{k_x \phi_{uu}(z_O^+; \lambda_x^+)}{U_\tau^2}\Big]}_{\text{spectrum of } \widehat{u}^+(z^+_{\max}, t^+)} d\ln(\lambda_x^+). \tag{11}$$

Here the integrand is the spectrum of the superposed fluctuations at $z^+_{\max}$, equating the spectrum of the outer-region fluctuations (spectrum at z_O^+) multiplied by the gain squared of the kernel ($|H_L|^2$ for $z^+_{\max}$ and z_O^+). When integrating the superposition spectrum over all scales we obtain the portion of the streamwise variance at $z^+_{\max}$ that is linearly coherent with z_O^+.

For a sequence of five Reynolds numbers [8], the premultiplied u-spectra at $z_O^+ \approx 3.9\mathrm{Re}_\tau^{1/2}$ are shown in Fig. 10; the three subfigures have an (a) outer scaling, (b) log scaling, and (c) inner scaling of the wavelength axes on the abscissae. In addition, superposition spectra are shown at the inner-peak location $z^+_{\max}$, alongside the gain squared of the linear transfer kernel, which is assumed to be fixed in inner scaling [one curve on Fig. 10(c)].

As is evident from Figs. 10(a)–10(c), the energy spectra do not collapse at the small wavelengths for any of the wavelength scalings where the velocity fluctuations are incoherent between z_O and $z_{\max}$ (i.e., where $|H_L|^2 \approx 0$). In fact, the energy residing at z_O^+ and at scales $\lambda_x^+ \lesssim 10^4$ decreases with increasing Re_τ [see Fig. 10(c)]. The large-scale energy content, on the other hand, residing at z_O^+ and at scales $\lambda_x^+ \gtrsim 10^4$, increases with Re_τ. Figures 11(a)–11(c) are similar to those in Fig 10, but now for an outer-region position that is fixed at $z_O^+ \approx 470$. Again, it is noted that where $|H_L|^2 \approx 0$, the small scales do not strictly collapse and there are small differences between the spectra for different Reynolds numbers. These small differences, however, are significant and strictly mean that the IOIM, as discussed in Sec. III B, cannot exactly reproduce the scaling of the inner-peak variance, in relation to the outer-region input.

Considering this further, we focus on Fig. 11(c) only and discuss a few open questions. The integrated energy content at z_O^+ and at the scales that are *coherent* with $z^+_{\max}$ (roughly at scales $\lambda_x^+ \gtrsim 10^4$, although this is properly resolved by coherence spectra as a scale-dependent weighting; recall Sec. II B) increases with Re_τ as $A_1^{\mathrm{C}} \ln(\mathrm{Re}_\tau)$. The superscript "C" here refers to coherent and A_1^{C} is likely larger than A_1, given that the integrated energy content that is *incoherent* with $z^+_{\max}$

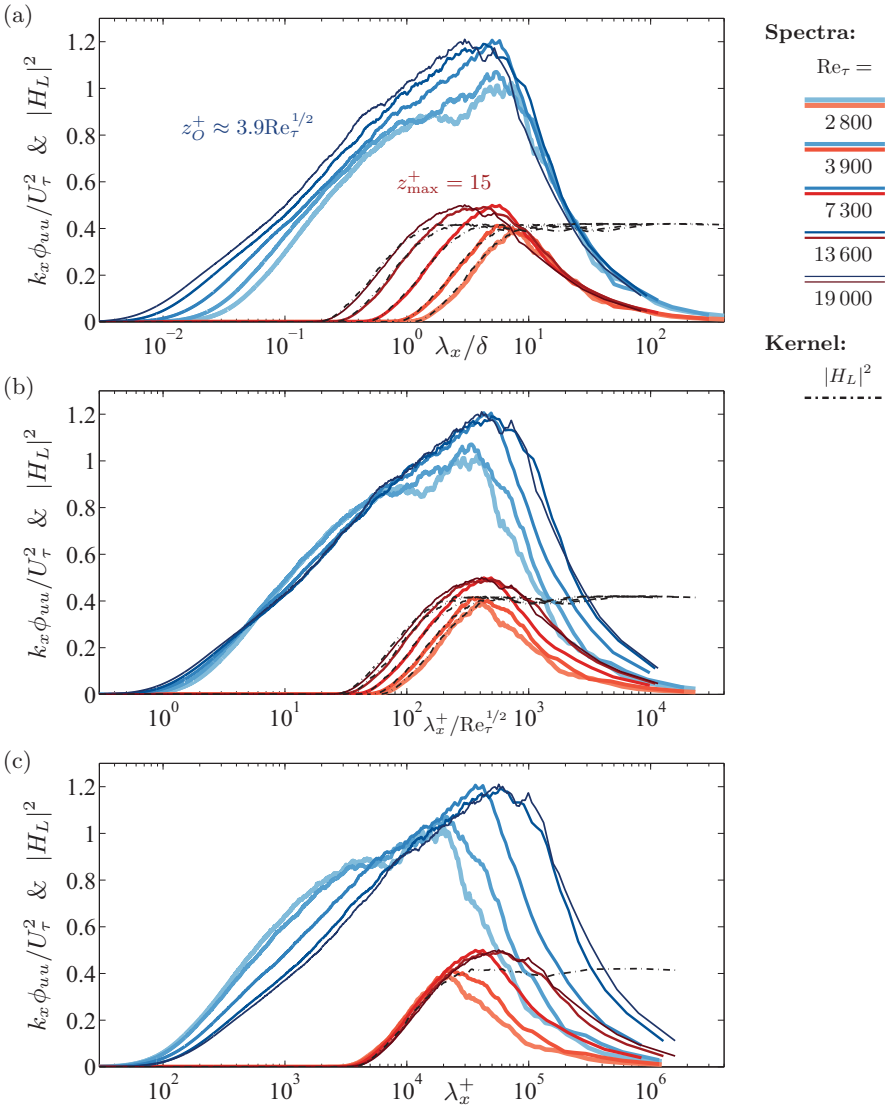

FIG. 10. Premultiplied spectra of the streamwise velocity fluctuations at an outer-region position $z_O^+ \approx 3.9\mathrm{Re}_\tau^{1/2}$ for five values of Re_τ. Alongside are the premultiplied spectra of the superposition IOIM component at $z_{\max}^+ = 15$, which equal the outer-region spectra multiplied by the gain squared of the kernel between $z_{\max}^+ = 15$ and z_O^+ (indicated with the dash-dotted line). The panels sequentially employ an (a) outer, (b) log, and (c) inner scaling of the wavelength axes on the abscissae.

(roughly $\lambda_x^+ \lesssim 10^4$) decreases with increasing Re_τ. Furthermore, we observe that the kernel at the coherent (large) scales plateaus to ~ 0.41. Consequently, the energy superimposed roughly scales as $0.41 A_1^C \ln(\mathrm{Re}_\tau)$ if one would accept the kernel to be universal for $z_O^+ \approx 470$ and $z_{\max}^+ = 15$. Given that the inner-peak variance scales as $0.63\ln(\mathrm{Re}_\tau)$, see Sec. III B, this would imply that $A_1^C \approx 0.63/0.41 \approx 1.54$. It is noted that this is different to the empirically reported result of $A_1 = 1.26$, and it remains an open question whether A_1 would be closer to 1.54 for data at much higher Reynolds numbers. (Interestingly, Kunkel and Marusic [82] reported $A_1 \approx 1.5$ from spectra in the atmospheric surface layer.) Further work is required to resolve these issues, and ideally requires

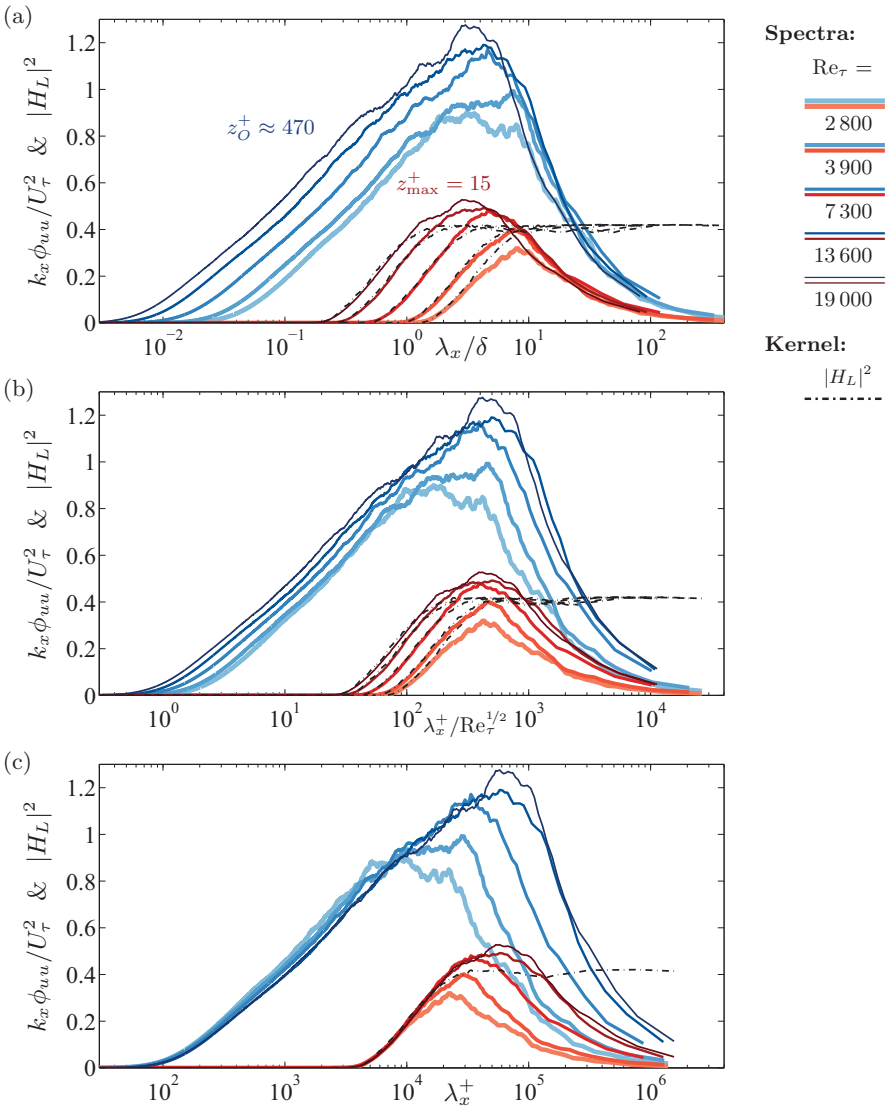

FIG. 11. Similar to Fig. 10 but now for $z_O^+ \approx 470$. Note that the gain squared of the kernel, $|H_L|^2$, is the same as in Fig. 10 and that this kernel was derived from a calibration experiment at $\mathrm{Re}_\tau \approx 13\,300$, for which $z_O^+ \approx 3.9\mathrm{Re}_\tau^{1/2} \approx 470$.

a spectral decomposition based on stochastically *coherent* and *incoherent* fluctuations between the inner and outer regions.

IV. CONCLUDING REMARKS

In this paper empirical scaling laws for the inner- and outer-region trends of the streamwise turbulence intensity have been considered in the light of inner-outer interactions. Wall-normal profiles of the u variance, acquired in Melbourne's boundary layer facility using hot-wire anemometry [78] and corrected for limited sensor resolution [79], are seen to follow $\overline{u^2}^+ = B_1 - A_1 \ln(z/\delta)$, with $A_1 \approx 1.26$ [49] in the logarithmic region, while the near-wall peak values at $z^+_{\max} \approx 15$ follow

$\overline{u^2}^+_{\max} = B_2 - A_2 \ln(z/\delta)$, with $A_2 \approx 0.63$, resulting in a Reynolds number dependence of the peak value via $\overline{u^2}^+_{\max} = C + A_2 \ln(\mathrm{Re}_\tau)$. The latter relation with $A_2 \approx 0.63$ has also been observed for DNS data [16,17,56] and describes boundary layer data taken at the Flow Physics Facility [81]. Note that empirically $A_2 = A_1/2$, suggesting that these scaling laws are related through an inner-outer interaction.

In high-Reynolds-number wall turbulence, inner-outer interactions are evident from energy spectra of the streamwise velocity fluctuations in the near-wall region. That is, small-scale turbulence in this region (or the portion of turbulence that is *not coherent* with the outer-region) may adhere to the classical description of near-wall turbulence, in which all inner-scaled turbulence statistics can be expressed as universal functions of z^+ (in this case $A_2 = 0$). However, when Re_τ grows, the energy in the outer region grows. Subsequently, outer-region fluctuations that are *coherent* with the near-wall region (referred to as "wall-attached") are superposed onto the near-wall turbulence. Hence, the peak variance of u grows with increasing Re_τ.

It is noted, however, that since only a portion of the outer-region fluctuations are coherent with the wall, the total streamwise turbulence intensity in the outer region comprises both wall-attached and wall-detached motions [1]. In Townsend's [5] attached eddy hypothesis, the logarithmic layer of wall turbulence solely consists of wall-attached, geometrically self-similar and inertia-dominated turbulent motions, and therefore they alone cannot fully describe the relation between the two aforementioned inner- and outer-scaling laws by solely focusing on the turbulence intensity (all scales lumped into a single variance). Whether, at extremely high Re_τ this portion of turbulence would dominate the spectrum remains an open question. What is clear is that the need exists for novel decomposition techniques to fully uncover: (1) the inner-scaled, universal portion of wall-bounded turbulence, (2) a portion that reflects pure attached eddies in the sense of Townsend (Reynolds number dependent and obeying inner and outer scalings), and (3) remaining portions that may still be Reynolds number dependent, such as the emergence of superstructures and very-large-scale motions. Unraveling the raw signature of wall turbulence, in which the classical view of universal-inner-scaled turbulence can coexist with Kolmogorov-type turbulence and Re-dependent contributions, such as the one conceptualized by Townsend, remains a rich area of research.

ACKNOWLEDGMENT

The authors gratefully acknowledge the financial support of the Australian Research Council.

[1] W. J. Baars, N. Hutchins, and I. Marusic, Self-similarity of wall-attached turbulence in boundary layers, J. Fluid Mech. **823**, R2 (2017).
[2] W. J. Baars, N. Hutchins, and I. Marusic, Spectral stochastic estimation of high-Reynolds-number wall-bounded turbulence for a refined inner-outer interaction model, Phys. Rev. Fluids **1**, 054406 (2016).
[3] N. Hutchins and I. Marusic, Evidence of very long meandering structures in the logarithmic region of turbulent boundary layers, J. Fluid Mech. **579**, 1 (2007).
[4] N. Hutchins and I. Marusic, Large-scale influences in near-wall turbulence, Phil. Trans. R. Soc. A **365**, 647 (2007).
[5] A. A. Townsend, *The Structure of Turbulent Shear Flow* (Cambridge University Press, Cambridge, 1976).
[6] A. E. Perry and M. S. Chong, On the mechanism of wall turbulence, J. Fluid Mech. **119**, 173 (1982).
[7] P. M. Ligrani and P. Bradshaw, Spatial resolution and measurement of turbulence in the viscous sublayer using subminiature hot-wire probes, Exp. Fluids **5**, 407 (1987).
[8] N. Hutchins, T. B. Nickels, I. Marusic, and M. S. Chong, Hot-wire spatial resolution issues in wall-bounded turbulence, J. Fluid Mech. **635**, 103 (2009).

[9] M. Hultmark, M. Vallikivi, S. C. C. Bailey, and A. J. Smits, Turbulent Pipe Flow at Extreme Reynolds Numbers, Phys. Rev. Lett. **108**, 094501 (2012).
[10] M. Vallikivi, M. Hultmark, and A. J. Smits, Turbulent boundary layer statistics at very high Reynolds number, J. Fluid Mech. **779**, 371 (2015).
[11] J. C. Klewicki and R. E. Falco, On accurately measuring statistics associated with small-scale structure in turbulent boundary layers using hot-wire probes, J. Fluid Mech. **219**, 119 (1990).
[12] D. B. DeGraaff and J. K. Eaton, Reynolds number scaling of the flat-plate turbulent boundary layer, J. Fluid Mech. **422**, 319 (2000).
[13] M. M. Metzger, J. C. Klewicki, K. L. Bradshaw, and R. Sadr, Scaling the near-wall axial turbulent stress in the zero pressure gradient boundary layer, Phys. Fluids **13**, 1819 (2001).
[14] M. M. Metzger and J. C. Klewicki, A comparative study of near-wall turbulence in high and low Reynolds number boundary layers, Phys. Fluids **13**, 692 (2001).
[15] I. Marusic and G. J. Kunkel, Streamwise turbulence intensity formulation for flat-plate boundary layers, Phys. Fluids **15**, 2461 (2003).
[16] S. Hoyas and J. Jiménez, Scaling of the velocity fluctuations in turbulent channels up to $Re_\tau = 2003$, Phys. Fluids **18**, 011702 (2006).
[17] M. Lee and R. D. Moser, Direct numerical simulation of turbulent channel flow up to $Re_\tau = 5200$, J. Fluid Mech. **774**, 395 (2015).
[18] R. Örlü, T. Fiorini, A. Segalini, G. Bellani, A. Talamelli, and P. H. Alfredsson, Reynolds stress scaling in pipe flow turbulence—First results from CICLoPE, Phil. Trans. R. Soc. A **375**, 20160187 (2017).
[19] H. Abe, H. Kawamura, and H. Choi, Very large-scale structures and their effects on the wall shear-stress fluctuations in a turbulent channel flow up to $Re_\tau = 640$, J. Fluids Eng. **126**, 835 (2004).
[20] J. Jiménez, J. C. del Álamo, and O. Flores, The large-scale dynamics of near-wall turbulence, J. Fluid Mech. **505**, 179 (2004).
[21] I. Marusic and N. Hutchins, Study of the log-layer structure in wall turbulence over a very large range of Reynolds number, Flow, Turbul. Combust. **81**, 115 (2008).
[22] S. J. Kline, W. C. Reynolds, F. A. Schraub, and P. W. Rundstadler, The structure of turbulent boundary layers, J. Fluid Mech. **30**, 741 (1967).
[23] S. J. Kline and S. K. Robinson, Quasi-coherent structures in the turbulent boundary layer: Part 1. Status report on a community wide summary of the data, in *Near-Wall Turbulence*, edited by S. J. Kline and N. H. Afghan (Hemisphere, 1988), p. 200.
[24] S. K. Robinson, Coherent motions in turbulent boundary layers, Annu. Rev. Fluid Mech. **23**, 601 (1991).
[25] J. Jiménez and A. Pinelli, The autonomous cycle of near-wall turbulence, J. Fluid Mech. **389**, 335 (1999).
[26] R. Mathis, I. Marusic, S. I. Chernyshenko, and N. Hutchins, Estimating wall-shear-stress fluctuations given an outer region input, J. Fluid Mech. **715**, 163 (2013).
[27] C. Zhang and S. I. Chernyshenko, Quasisteady quasihomogeneous description of the scale interactions in near-wall turbulence, Phys. Rev. Fluids **1**, 014401 (2016).
[28] L. Agostini and M. Leschziner, On the validity of the quasi-steady-turbulence hypothesis in representing the effects of large scales on small scales in boundary layers, Phys. Fluids **28**, 045102 (2016).
[29] W. J. Baars, N. Hutchins, and I. Marusic, Reynolds number trend of hierarchies and scale interactions in turbulent boundary layers, Phil. Trans. R. Soc. A **375**, 20160077 (2017).
[30] I. Marusic, R. Mathis, and N. Hutchins, Predictive model for wall-bounded turbulent flow, Science **329**, 193 (2010).
[31] R. Mathis, N. Hutchins, and I. Marusic, A predictive inner–outer model for streamwise turbulence statistics in wall-bounded flows, J. Fluid Mech. **681**, 537 (2011).
[32] J. Jiménez, Cascades in wall-bounded turbulence, Annu. Rev. Fluid Mech. **44**, 27 (2012).
[33] O. Flores and J. Jiménez, Hierarchy of minimal flow units in the logarithmic layer, Phys. Fluids **22**, 071704 (2010).
[34] Y. Hwang, Statistical structure of self-sustaining attached eddies in turbulent channel flow, J. Fluid Mech. **767**, 254 (2015).
[35] W. Schoppa and F. Hussain, Coherent structure generation in near-wall turbulence, J. Fluid Mech. **453**, 57 (2002).

[36] J. Klewicki, P. Fife, and T. Wei, On the logarithmic mean profile, J. Fluid Mech. **638**, 73 (2009).
[37] B. J. McKeon, The engine behind (wall) turbulence: Perspectives on scale interactions, J. Fluid Mech. **817**, P1 (2017).
[38] L. Hellström, I. Marusic, and A. J. Smits, Self-similarity of the large-scale motions in turbulent pipe flow, J. Fluid Mech. **792**, R1 (2016).
[39] X. Wu and P. Moin, Direct numerical simulation of turbulence in a nominally-zero-pressure-gradient flat-plate boundary layer, J. Fluid Mech. **630**, 5 (2009).
[40] Y. Jodai and G. E. Elsinga, Experimental observation of hairpin auto-generation events in a turbulent boundary layer, J. Fluid Mech. **795**, 611 (2016).
[41] C. M. de Silva, N. Hutchins, and I. Marusic, Uniform momentum zones in turbulent boundary layers, J. Fluid Mech. **786**, 309 (2016).
[42] C. M. de Silva, J. Philip, N. Hutchins, and I. Marusic, Interfaces of uniform momentum zones in turbulent boundary layers, J. Fluid Mech. **820**, 451 (2017).
[43] R. J. Adrian, C. D. Meinhart, and C. D. Tomkins, Vortex organization in the outer region of the turbulent boundary layer, J. Fluid Mech. **422**, 1 (2000).
[44] P. J. A. Priyadarshana, J. C. Klewicki, S. Treat, and J. F. Foss, Statistical structure of turbulent-boundary-layer velocity—Vorticity products at high and low Reynolds numbers, J. Fluid Mech. **570**, 307 (2007).
[45] J. Eisma, J. Westerweel, G. Ooms, and G. E. Elsinga, Interfaces and internal layers in a turbulent boundary layer, Phys. Fluids **27**, 055103 (2015).
[46] M. V. Zagarola and A. J. Smits, Mean-flow scaling of turbulent pipe flow, J. Fluid Mech. **373**, 33 (1998).
[47] H. M. Nagib, K. A. Chauhan, and P. A. Monkewitz, Approach to an asymptotic state for zero pressure gradient turbulent boundary layers, Phil. Trans. R. Soc. A **365**, 755 (2007).
[48] I. Marusic, B. J. McKeon, P. A. Monkewitz, H. M. Nagib, A. J. Smits, and K. R. Sreenivasan, Wall-bounded turbulent flows: Recent advances and key issues, Phys. Fluids **22**, 065103 (2010).
[49] I. Marusic, J. P. Monty, M. Hultmark, and A. J. Smits, On the logarithmic region in wall turbulence, J. Fluid Mech. **716**, R3 (2013).
[50] K. R. Sreenivasan and A. Sahay, The persistence of viscous effects in the overlap region and the mean velocity in turbulent pipe and channel flows, in *Self-Sustaining Mechanisms of Wall Turbulence*, edited by R. Panton (Computational Mechanics Publications, Southampton, UK and Boston, USA, 1997), p. 253.
[51] I. Marusic, R. Mathis, and N. Hutchins, High Reynolds number effects in wall turbulence, Int. J. Heat Fluid Flow **31**, 418 (2010).
[52] A. J. Smits, B. J. McKeon, and I. Marusic, High Reynolds number wall turbulence, Annu. Rev. Fluid Mech. **43**, 353 (2011).
[53] A. E. Perry, I. Marusic, and M. B. Jones, On the streamwise evolution of turbulent boundary layers in arbitrary pressure gradients, J. Fluid Mech. **461**, 61 (2002).
[54] N. Renard and S. Deck, A theoretical decomposition of mean skin friction generation into physical phenomena across the boundary layer, J. Fluid Mech. **790**, 339 (2016).
[55] B. J. Cantwell, Organized motion in turbulent flow, Annu. Rev. Fluid Mech. **13**, 457 (1981).
[56] J. A. Sillero, J. Jiménez, and R. D. Moser, One-point statistics for turbulent wall-bounded flows at Reynolds numbers up to $\delta^+ \approx 2000$, Phys. Fluids **25**, 105102 (2013).
[57] I. Marusic and W. D. C. Heuer, Reynolds Number Invariance of the Structure Inclination Angle in Wall Turbulence, Phys. Rev. Lett. **99**, 114504 (2007).
[58] R. J. Adrian, Conditional eddies in isotropic turbulence, Phys. Fluids **22**, 2065 (1979).
[59] C. E. Tinney, F. Coiffet, J. Delville, M. N. Glauser, P. Jordan, and A. M. Hall, On spectral linear stochastic estimation, Exp. Fluids **41**, 763 (2006).
[60] K. Chauhan, N. Hutchins J. Monty, and I. Marusic, Structure inclination angles in the convective atmospheric surface layer, Boundary-Layer Meteorol. **147**, 41 (2013).
[61] R. Mathis, N. Hutchins, and I. Marusic, Large-scale amplitude modulation of the small-scale structures in turbulent boundary layers, J. Fluid Mech. **628**, 311 (2009).
[62] W. Sidebottom, O. Cabrit, I. Marusic, C. Meneveau, A. Ooi, and D. Jones, Modelling of wall shear-stress fluctuations for large-eddy simulation, in *Proceedings of the 19th Australasian Fluid Mechanics Conference* (Melbourne, Australia, 2014).

[63] R. J. Adrian and P. Moin, Stochastic estimation of organized turbulent structure: Homogeneous shear flow, J. Fluid Mech. **190**, 531 (1988).
[64] Y. G. Guezennec, Stochastic estimation of coherent structures in turbulent boundary layers, Phys. Fluids A **1**, 1054 (1989).
[65] J. P. Bonnet, D. R. Cole, J. Delville, M. N. Glauser, and L. S. Ukeiley, Stochastic estimation and proper orthogonal decomposition: Complementary techniques for identifying structure, Exp. Fluids **17**, 307 (1994).
[66] K. T. Christensen and R. J. Adrian, Statistical evidence of hairpin vortex packets in wall turbulence, J. Fluid Mech. **431**, 433 (2001).
[67] A. M. Naguib, C. E. Wark, and O. Juckenhöfel, Stochastic estimation and flow sources associated with surface pressure events in a turbulent boundary layer, Phys. Fluids **13**, 2611 (2001).
[68] M. Stanislas, L. Perret, and J.-M. Foucaut, Vortical structures in the turbulent boundary layer: A possible route to a universal representation, J. Fluid Mech. **602**, 327 (2008).
[69] F. Kerhervé, S. Roux, and R. Mathis, Combining time-resolved multi-point and spatially-resolved measurements for the recovering of very-large-scale motions in high Reynolds number turbulent boundary layer, Exp. Therm. Fluid Sci. **82**, 102 (2017).
[70] J. C. del Álamo and J. Jiménez, Linear energy amplification in turbulent channels, J. Fluid Mech. **559**, 205 (2006).
[71] P. R. Bandyopadhyay and A. K. M. F. Hussain, The coupling between scales in shear flows, Phys. Fluids **27**, 2221 (1984).
[72] W. J. Baars, K. M. Talluru, N. Hutchins, and I. Marusic, Wavelet analysis of wall turbulence to study large-scale modulation of small scales, Exp. Fluids **56**, 188 (2015).
[73] L. Agostini, M. Leschziner, and D. Gaitonde, Skewness-induced asymmetric modulation of small-scale turbulence by large-scale structures, Phys. Fluids **28**, 015110 (2016).
[74] D. T. Squire, W. J. Baars, N. Hutchins, and I. Marusic, Inner–outer interactions in rough-wall turbulence, J. Turbulence **17**, 1159 (2016).
[75] Model calibration parameters with a complementary MATLAB script for performing model predictions are available for download at http://fluids.eng.unimelb.edu.au/#data.
[76] P. H. Alfredsson, A. Segalini, and R. Örlü, A new scaling for the streamwise turbulence intensity in wall-bounded turbulent flows and what it tells us about the "outer" peak, Phys. Fluids **23**, 041702 (2016).
[77] P. A. Monkewitz and H. M. Nagib, Large Reynolds number asymptotics of the stream-wise normal stress in ZPG turbulent boundary layers, J. Fluid Mech. **783**, 474 (2015).
[78] I. Marusic, K. A. Chauhan, V. Kulandaivelu, and N. Hutchins, Evolution of zero-pressure-gradient boundary layers from different tripping conditions, J. Fluid Mech. **783**, 379 (2015).
[79] A. J. Smits, J. Monty, M. Hultmark, S. C. C. Bailey, N. Hutchins, and I. Marusic, Spatial resolution correction for wall-bounded turbulence measurements, J. Fluid Mech. **676**, 41 (2011).
[80] J. C. Klewicki, Reynolds number dependence, scaling, and dynamics of turbulent boundary layers, J. Fluids Eng. **132**, 094001 (2010).
[81] P. Vincenti, J. C. Klewicki, C. Morrill-Winter, C. M. White, and M. Wosnik, Streamwise velocity statistics in turbulent boundary layers that spatially develop to high Reynolds number, Exp. Fluids **54**, 1 (2013).
[82] G. J. Kunkel and I. Marusic, Study of the near-wall-turbulent region of the high-Reynolds-number boundary layer using an atmospheric flow, J. Fluid Mech. **548**, 375 (2006).